CHEMISTRY OF MATERIALS

pubs.acs.org/cm

Article

Effectiveness of Different Ligands on Silane Precursors for Ligand Exchange to Etch Metal Fluorides

Ann Lii-Rosales, Virginia L. Johnson, Andrew S. Cavanagh, Andreas Fischer, Thorsten Lill, Sandeep Sharma, and Steven M. George*

Cite This: *Chem. Mater.* 2022, 34, 8641−8653

Read Online

ACCESS | Metrics & More | Article Recommendations | Supporting Information

ABSTRACT: Metal fluorides can be spontaneously etched by ligand-exchange reactions. During these reactions, the exchange of ligands between the incoming precursor and the metal fluoride leads to the volatilization of the metal fluoride. These ligand-exchange reactions are important in many thermal atomic layer etching (ALE) processes. To test the effectiveness of different ligands for ligand exchange, the spontaneous etching of metal fluorides by silane precursors containing different ligands was investigated using *in situ* quadrupole mass spectrometry (QMS). The homoleptic and heteroleptic silane precursors were $SiCl_4$, $SiCl_2(CH_3)_2$, $SiCl(CH_3)_2H$, and $Si(CH_3)_4$. These silane precursors provide Cl, CH_3, or H ligands for the ligand-exchange reaction. The metal fluorides were GaF_3, InF_3, ZnF_2, ZrF_4, HfF_4, and SnF_4. The QMS results showed that F/Cl ligand exchange was observed for all the metal fluorides with chlorine-containing silane precursors. In addition, all the volatile metal etch products were metal chlorides, namely, $GaCl_3$, $InCl_3$, $ZnCl_2$, $ZrCl_4$, $HfCl_4$, and $SnCl_4$. No metal methyl complexes were detected as volatile metal etch products indicating no F/CH_3 exchange. For $SiCl(CH_3)_2H$ as the silane precursor, the observation of $SiF_2(CH_3)_2$ indicated that F/H exchange is also possible in addition to F/Cl exchange. For the various metal fluorides, the dominance of the F/Cl exchange led to nearly equivalent onset temperatures for ligand exchange and for etching to yield metal chlorides. Thermochemical calculations of the ligand-exchange reactions also predicted the formation of metal chlorides. All F/Cl exchanges were the most thermodynamically favorable as demonstrated by their negative changes in Gibbs free energy (ΔG). These experimental and theoretical results provide guidelines for designing precursors for thermal ALE processes.

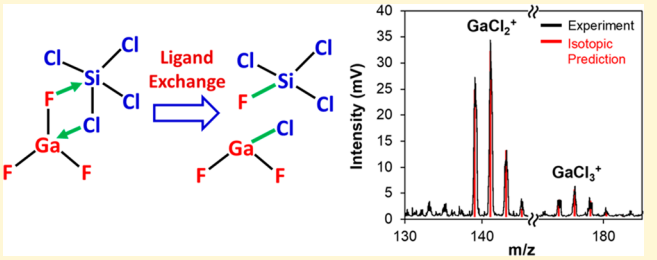

1. INTRODUCTION

Thermal atomic layer etching (ALE) is a gas phase etching technique that utilizes sequential and self-limiting surface reactions.[1,2] The reactions consist of a surface modification step followed by volatile release of the modified surface.[1,2] For the thermal ALE of metal oxides such as Al_2O_3, HfO_2, and ZrO_2, the modification step typically involves fluorination using HF.[2−11] The volatile release step can then employ a ligand-exchange reaction that can be characterized as a transmetalation reaction.[12] During the ligand-exchange reaction, the ligands on the precursor are exchanged with the F ligands in the metal fluoride.

Various precursors have been demonstrated for ligand exchange in thermal ALE such as $Al(CH_3)_3$, $AlCl(CH_3)_2$, $SiCl_4$, $TiCl_4$, BCl_3, $Ga(N(CH_3)_2)_3$, and $Sn(acac)_2$.[1−11,13,14] Most of these precursors contain ligands such as Cl and CH_3. These are effective ligands for volatile release if the reaction can produce stable and volatile metal chlorides or metal methyl complexes. Out of the various precursors demonstrated for ligand exchange in thermal ALE, only $SiCl_4$ is a silane precursor.[8] Silanes are an important class of precursors for ligand exchange with metal fluorides because of strong Si−F covalent bonding.[15] The Si−F bond formation can be a substantial thermochemical driving force for ligand exchange. In addition, Si can form complexes with a wide variety of ligands. Consequently, silane precursors containing different ligands are an excellent testbed for exploring the effectiveness of various ligands for ligand exchange in thermal ALE.

This work explores the spontaneous etching of metal fluorides with silane precursors. The spontaneous etching models the volatile release of the surface fluoride in thermal ALE. The spontaneous etching reactions were studied using a reactor equipped with sample heating and *in situ* quadrupole mass spectrometry (QMS).[16] Six different metal fluorides were studied including GaF_3, InF_3, ZnF_2, ZrF_4, HfF_4, and SnF_4. These metal fluorides represent the corresponding metal oxides after fluorination in the surface modification step during

Received: May 28, 2022
Revised: September 2, 2022
Published: September 19, 2022

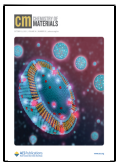

Downloaded via UNIV OF COLORADO BOULDER on October 11, 2022 at 23:09:23 (UTC).
See https://pubs.acs.org/sharingguidelines for options on how to legitimately share published articles.

ACS Publications

© 2022 American Chemical Society

thermal ALE. Four different homoleptic and heteroleptic silane precursors were explored for ligand exchange including $SiCl_4$, $SiCl_2(CH_3)_2$, $SiCl(CH_3)_2H$, and $Si(CH_3)_4$. These silane precursors are shown in Figure 1. Only $SiCl_4$, together with HF for fluorination, has been previously employed for ligand exchange during the thermal ALE of HfO_2 and ZrO_2.[8]

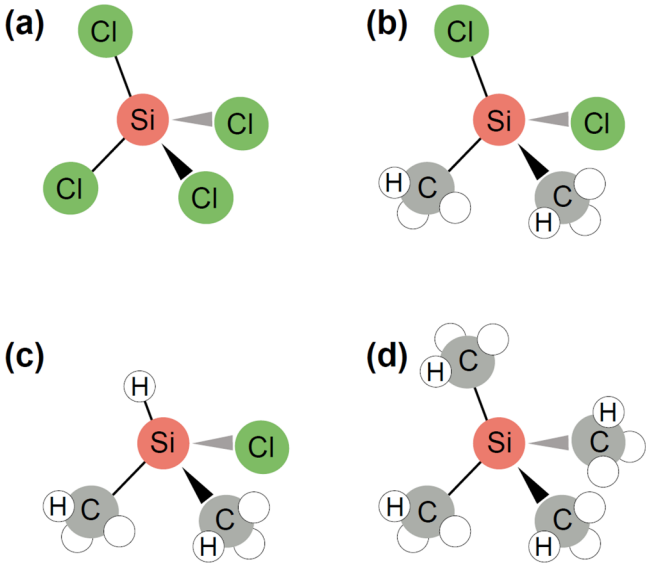

Figure 1. Pictures of the silane precursors: (a) $SiCl_4$ (silicon tetrachloride), (b) $SiCl_2(CH_3)_2$ (dichlorodimethyl-silane), (c) $SiCl(CH_3)_2H$ (chlorodimethyl-silane), and (d) $Si(CH_3)_4$ (tetramethyl-silane).

The various silane precursors allow the F/Cl, F/CH_3, and F/H exchange reactions to be studied by monitoring the ligand-exchange and metal etch products using *in situ* QMS investigations.[16] The relative importance of F/Cl, F/CH_3, and F/H exchange reactions can be determined by measuring the intensity of the ligand-exchange and metal etch products and their temperature dependence. In addition, the ligand-exchange reactions must be thermodynamically favorable to generate stable and volatile products. Thermochemical calculations were performed to determine the change in Gibbs free energy (ΔG) for each combination of the different silane precursors with the various metal fluorides. These experimental and theoretical studies help to clarify the importance of the specific ligand during ligand-exchange reactions. This understanding is also useful for the design of effective reactants for thermal ALE.

2. EXPERIMENTAL SECTION

2.1. Quadrupole Mass Spectrometry (QMS) Reactor. Detection of volatile species during the ligand-exchange reactions was accomplished using a reactor equipped with *in situ* QMS (Extrel, MAX-QMS Flange Mounted System).[16] The QMS reactor was also equipped with a sample housing that could be heated to obtain a temperature ramp.[16] Typical temperature ramps were 3 °C/min and ranged from room temperature at 20 °C to a limiting temperature of 530 °C. All volatile species were entrained in a N_2 molecular beam and delivered line-of-sight to the QMS ionizer entrance.[16] This configuration allowed for direct and accurate analysis of the volatile species.

The metal fluoride powder was placed in the sample housing. N_2 was flowed through the sample housing together with the silane precursors.[16] The typical operating pressure inside the sample housing was 2−3 Torr under the N_2 viscous flow. The pressure in the differentially pumped area outside the sample housing was in the low 10^{-5} Torr range. The differentially pumped QMS chamber was in the low 10^{-7} to high 10^{-8} Torr range. Additional details of the QMS reactor have been reported previously.[16]

2.2. Chemicals for Ligand-Exchange Reactions. Metal fluoride powders used in the ligand-exchange reactions included GaF_3 (anhydrous, 99.85%, Alfa Aesar), InF_3 (≥99.9%, Sigma-Aldrich), ZnF_2 (anhydrous, 99%, Strem Chemicals), ZrF_4 (99.9%, Sigma-Aldrich), HfF_4 (99.9%, Sigma-Aldrich), and SnF_4 (Sigma-Aldrich). The masses of the metal fluoride powders placed in the sample housing were between 0.05 and 0.10 g.

The silane precursors for ligand exchange included both homoleptic and heteroleptic silane precursors. The homoleptic silane precursors were $SiCl_4$ (99%, Sigma-Aldrich) and $Si(CH_3)_4$ (99+%, Gelest). The heteroleptic silane precursors were $SiCl_2(CH_3)_2$ (≥99.5%, Sigma-Aldrich) and $SiCl(CH_3)_2H$ (98%, Sigma-Aldrich). The silane precursors were employed at room temperature. The partial pressures of the silane precursors in the sample housing ranged from 0.05 to 0.20 Torr. These pressures were present continuously during the temperature ramps.

In addition to their ability to perform ligand-exchange reactions, the various silane precursors could be employed for chemical vapor deposition (CVD) at higher temperatures. For example, $SiCl_4$ together with H_2 can be used for Si CVD at >800 °C.[17,18] Chloromethylsilanes like $SiCl_3(CH_3)$ can be utilized for SiC CVD at >1200 °C.[19] There have also been reports for thermal pyrolysis of $SiCl_2(CH_3)_2$ at >1000 °C.[20] These possible reactions are unlikely at the lower temperatures explored for ligand exchange. The QMS analysis also observed no evidence for products from CVD or thermal pyrolysis reactions at the temperatures < 530 °C employed for ligand exchange.

2.3. Computational Details. The thermodynamics of sequential ligand exchanges between the silane precursors and the metal fluorides was calculated using *ab initio* methods. Geometries and harmonic vibrational frequencies were calculated at the UB3LYP/Def2TZVP level of theory.[21,22] These calculations were followed by single-point energy calculations at a higher level of theory, UCCSD/sdd.[23−25]

Translational, vibrational, and rotational degrees of freedom, along with UCCSD single-point energies, were used to calculate the Gibbs free energies at 350 °C. An in-depth discussion of these thermochemical methods has been described earlier.[26] Gaussian 16 was used for all quantum chemical calculations.[27] Optimizations were performed with Gaussian's opt = tight, enforcing a root mean squared force criterion within 10^{-6} au. All geometries used in this work were optimized within 100 cycles.

ΔG was computed using $\Delta G = \Delta H - T\Delta S$. ΔH was calculated as the difference between the enthalpy of the product, $[H(T) - H(0)]_{prod}$ and the enthalpy of the reactant, $[H(T) - H(0)]_{reac}$. $H(0)$ is the enthalpy at zero temperature. $[H(T) - H(0)]$ is calculated using the expression

$$[H(T) - H(0)]_{reac/prod} = \frac{5}{2}k_B T + \sum_{\nu_i} \frac{h\nu_i}{\exp\left(\frac{h\nu_i}{k_B T}\right) - 1} + \frac{3}{2}k_B T \quad (1)$$

The translational, vibrational, and rotational contributions are represented by the three terms, respectively, in eq 1. All three terms include the Boltzmann constant, k_B, and temperature, T. The vibrational term contains contributions from all vibrational frequencies, ν_i, that are obtained using UB3LYP/Def2TZVP calculations, and h is Planck's constant.

The entropies of the product, S_{prod}, and the reactant, S_{reac}, are similarly calculated using

https://doi.org/10.1021/acs.chemmater.2c01603
Chem. Mater. 2022, 34, 8641−8653

$$S_{\mathrm{reac/prod}} = \left[k_B \ln\left(\left(\frac{2\pi m k_B T}{h^2}\right)^{3/2} V\right)\right] + \sum_{\nu_i}\left[-k_B \ln\left(1 - \exp\left(-\left(\frac{h\nu_i}{k_B T}\right)\right)\right) + \frac{h\nu_i}{T(\exp(h\nu_i/k_B T) - 1)}\right] + \left[\frac{3}{2}k_B + k_B \ln\left(\frac{\sqrt{\pi}}{\sigma_{\mathrm{ext}}}\prod_i \frac{8\pi^2 I_i k_B T}{h^2}\right)^{1/2}\right] \quad (2)$$

The translational, vibrational, and rotational contributions are separated as the first, second, and third terms, respectively, in eq 2. m is the mass of the species in question, V is the volume, σ_{ext} represents the molecule's external symmetry number, and the principle moments of inertia are given as I_i.

3. RESULTS AND DISCUSSION

3.1. Homoleptic $SiCl_4$ Precursor with Only Cl Ligands.

$SiCl_4$ (silicon tetrachloride) is a homoleptic silane precursor that is ideal for the study of F/Cl ligand exchange between Cl in $SiCl_4$ and F in metal fluorides. In addition, $SiCl_4$ has been used previously as a ligand-exchange precursor for the thermal ALE of ZrO_2 and HfO_2.[8]

3.1.A. GaF_3. GaF_3 powder was chosen to model Ga_2O_3 after fluorination by HF in the surface modification step during thermal ALE.[13] Ga_2O_3 thermal ALE has been previously reported using HF for fluorination and BCl_3, $Al(CH_3)_3$, $AlCl(CH_3)_2$, and $Ga(N(CH_3)_2)_3$ as ligand-exchange precursors for volatile release.[13] There have been no reports of Ga_2O_3 thermal ALE using $SiCl_4$ as the ligand-exchange precursor.

During $SiCl_4$ exposure to the GaF_3 powder at 375 °C, QMS measurements displayed in Figure 2 observed ion intensities

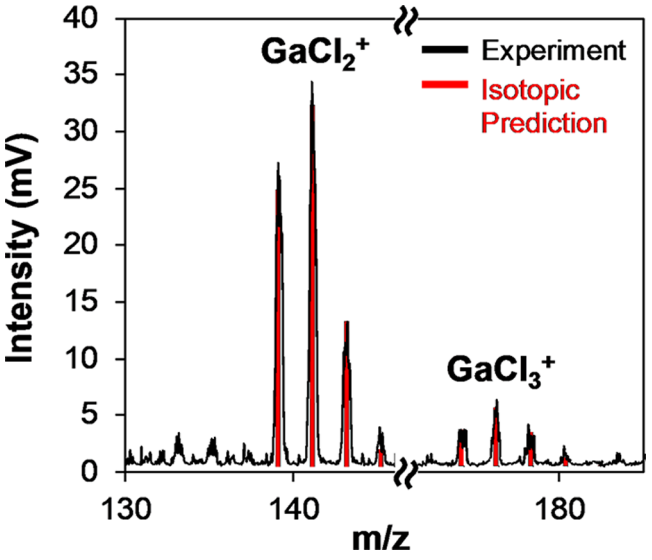

Figure 2. Mass spectrum showing ion intensities of $GaCl_3^+$ and $GaCl_2^+$ during the ligand-exchange reaction between $SiCl_4$ and GaF_3 powder at 375 °C.

for $GaCl_3^+$ at m/z values of 174, 176, 178, and 180. Under electron impact ionization, $GaCl_3$ also fragmented into $GaCl_2^+$ with ion intensities at m/z values of 139, 141, 143, and 145.[28] These species were identified by the isotopic fingerprints of ^{69}Ga, ^{71}Ga, ^{35}Cl, and ^{37}Cl. The isotopic prediction and experimental mass spectrum are in excellent agreement as depicted in Figure 2. The full mass spectrum from m/z 80–190 is given in Figure S1 in the Supporting Information. The observation of $GaCl_3^+$ in the gas phase indicates complete F/Cl exchange between $SiCl_4$ and GaF_3 to produce $GaCl_3$ as a volatile etch product. The observation of $GaCl_3$ indicates that the thermal ALE of Ga_2O_3 should be possible using HF for fluorination and $SiCl_4$ as the ligand-exchange precursor for volatile release.

The temperature dependence of the reaction between $SiCl_4$ and GaF_3 powder is shown in Figure 3. The $SiCl_3^+$ ion signal in

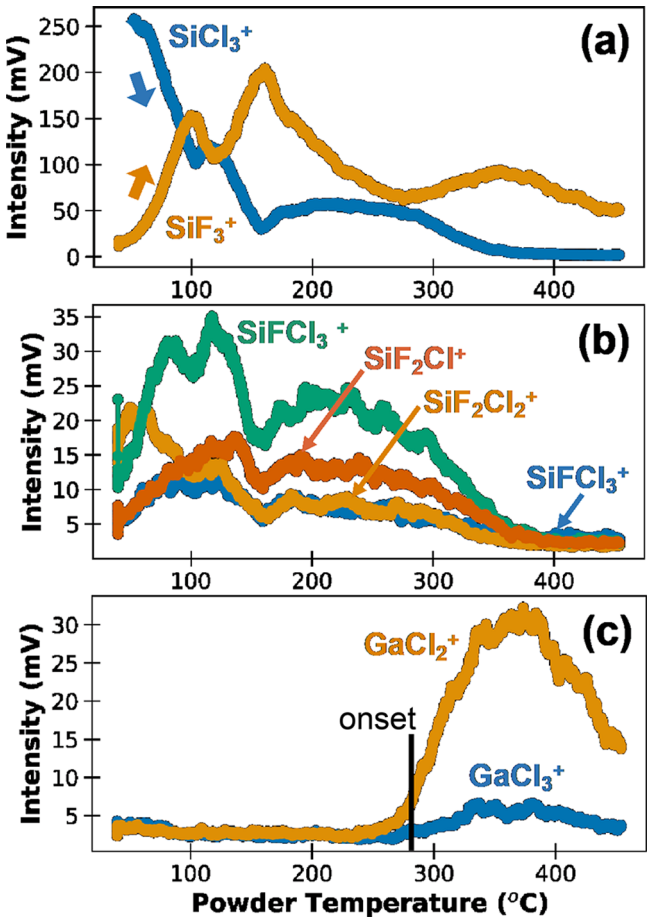

Figure 3. Ion intensities versus powder temperature during reaction between $SiCl_4$ and GaF_3 powder. (a) $SiCl_4$ precursor ($SiCl_3^+$) and SiF_4 ligand-exchange product (SiF_3^+) after complete F/Cl exchange. (b) Various $SiF_xCl_y^+$ species from partial F/Cl exchange. (c) $GaCl_3$ metal etch product ($GaCl_3^+$) and its fragment $GaCl_2^+$. The most intense isotope peak of each ion species is utilized in the plots.

Figure 3a is the largest signal after ionization of the $SiCl_4$ precursor.[29] As the temperature increased during the temperature ramp, the $SiCl_3^+$ ion intensity was observed to decrease progressively. Concurrently, the SiF_3^+ ion signal increased and exhibited a complementary behavior to the $SiCl_3^+$ ion signal. SiF_3^+ is the main ion signal after ionization of SiF_4.[30] Total F/Cl exchange between the $SiCl_4$ precursor and the GaF_3 surface produces SiF_4. Furthermore, the reciprocal relationship between the $SiCl_3^+$ and SiF_3^+ ion signals indicates that the dominant reaction pathway is complete F/Cl exchange.

Figure 3b shows that partial F/Cl exchange was also observed between $SiCl_4$ and the GaF_3 powder. However, the ion intensities for the various $SiF_xCl_y^+$ species are much lower than for SiF_3^+ in Figure 3a. The $SiF_xCl_y^+$ ion signals had a maximum intensity of 35 mV. In contrast, the SiF_3^+ ion signal

https://doi.org/10.1021/acs.chemmater.2c01603
Chem. Mater. 2022, 34, 8641−8653

had a maximum intensity of 200 mV. In addition, the $SiF_xCl_y^+$ ion signals did not exhibit a strong correlation with the $SiCl_3^+$ ion signal.

Figure 3c shows the results for the $GaCl_2^+$ and $GaCl_3^+$ ion intensities at m/z values of 141 and 176, respectively. These signals are from $GaCl_3$, the volatile metal etch product.[28] The presence of $GaCl_3$ indicates full F/Cl exchange. The $GaCl_3^+$ and $GaCl_2^+$ ion signals had an onset temperature of 285 °C. The onset temperature is the lowest temperature where the correct isotopic fingerprints are first observed for a given etch species. In comparison, the SiF_3^+ ion intensity was observed at temperatures as low as 55 °C. These results illustrate that ligand-exchange products can be observed at a much lower temperature than the metal etch products. Similar observations for ligand exchange with metal fluorides occurring at lower temperatures than the volatile metal etch products were reported earlier.[16]

These results suggest that F/Cl exchange leads to the buildup of Cl in the GaF_3 powder. A certain amount of Cl may be required in the GaF_3 powder before $GaCl_3$ can be released to the gas phase. $GaCl_3$ has a vapor pressure of 0.1 Torr at 25 °C.[31] If $GaCl_3$ was formed earlier during the temperature ramp, $GaCl_3$ should be desorbed and observed at temperatures below its onset temperature at 285 °C. During thermal ALE of Ga_2O_3 or GaN, the metal fluoride would only exist on the surface of Ga_2O_3 or GaN. The Cl from ligand exchange would not be diluted in a reservoir of metal fluoride. Consequently, the $GaCl_3$ etch products should appear at a lower onset temperature than in these experiments on metal fluoride powders.

3.1.B. ZnF_2. ZnF_2 powder models the fluorinated ZnO surface during thermal ALE.[32] ZnO thermal ALE has been previously reported using HF for fluorination and $Al(CH_3)_3$ as the ligand-exchange precursor for volatile release.[32] There have been no reports of ZnO thermal ALE using $SiCl_4$ as the ligand-exchange precursor. The reaction between $SiCl_4$ and ZnF_2 powder at 475 °C produced $ZnCl_2^+$ ion signals as displayed in Figure 4. $ZnCl_2^+$ is the parent molecular ion of $ZnCl_2$.[33] The appearance of $ZnCl_2^+$ ion signals indicates F/Cl exchange between the $SiCl_4$ precursor and the ZnF_2 surface. The isotopic prediction (red lines) shown in Figure 4 has an excellent match to the experimental mass spectrum of $ZnCl_2$ at m/z values of 134−143 amu. The full mass spectrum from m/z 60−150 is given in Figure S2 in the Supporting Information. The observation of $ZnCl_2^+$ ion intensity suggests that ZnO thermal ALE using HF for fluorination and $SiCl_4$ for volatile release should be feasible.

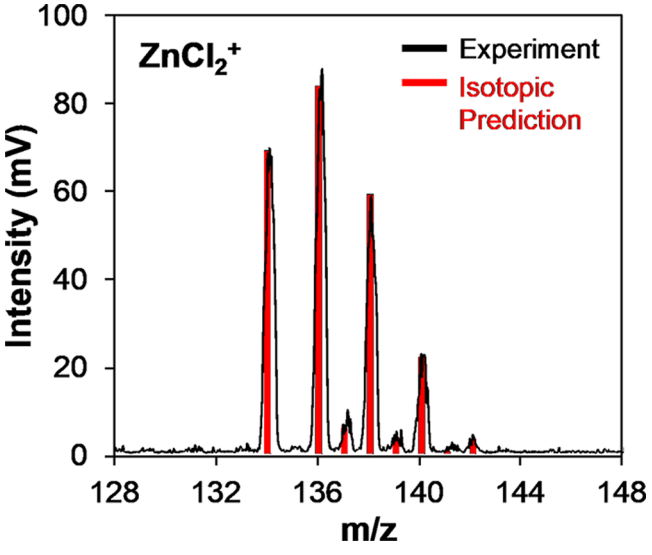

Figure 4. Mass spectrum showing ion intensities of $ZnCl_2^+$ during the ligand-exchange reaction between $SiCl_4$ and ZnF_2 powder at 475 °C.

The temperature dependence of the reaction between $SiCl_4$ and ZnF_2 powder is shown in Figure 5. As the $SiCl_3^+$ ion intensity decreased progressively with temperature in Figure 5a, the SiF_3^+ ion intensity increased in a complementary fashion with an onset temperature of 250 °C. This behavior demonstrates F/Cl exchange between $SiCl_4$ and ZnF_2. Figure 5b shows that the $ZnCl_2^+$ ion signal, representing the metal etch product, has an onset temperature at 325 °C. The observation of $ZnCl_2^+$ ion signal at only a slightly higher temperature than the onset temperature for ligand exchange indicates that F/Cl exchange readily forms a volatile $ZnCl_2$ etch product.

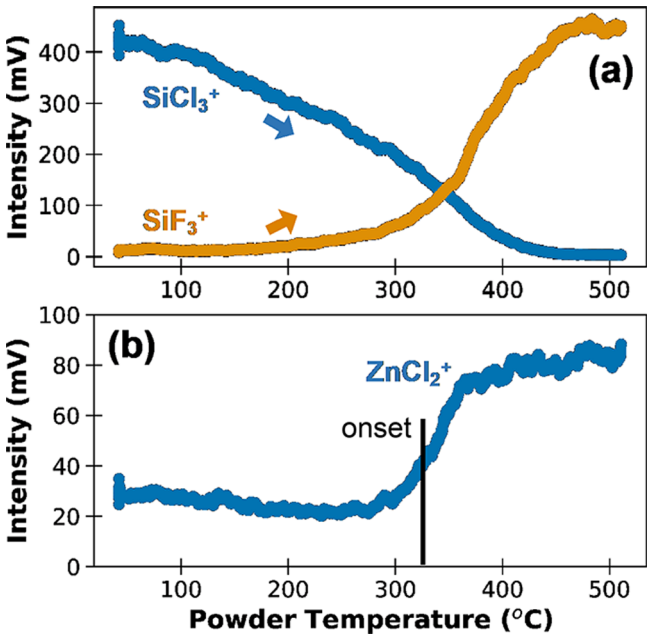

Figure 5. Ion intensities versus powder temperature during the reaction between $SiCl_4$ and ZnF_2 powder. (a) $SiCl_4$ precursor ($SiCl_3^+$) and SiF_4 ligand-exchange product (SiF_3^+) after total F/Cl exchange. (b) $ZnCl_2$ metal etch product ($ZnCl_2^+$). The most intense isotope peak of each ion species is shown in the plots.

3.1.C. ZrF_4. ZrF_4 powder models the fluorinated ZrO_2 surface in thermal ALE. ZrO_2 thermal ALE has been previously reported using HF for fluorination and $AlCl(CH_3)_2$, $SiCl_4$, and $TiCl_4$ as the ligand-exchange precursors for volatile release.[6−8] Various ion signals containing Zr were observed during $SiCl_4$ exposure to ZrF_4 powder at 450 °C. Figure 6 shows the most intense ion signals assigned to $ZrFCl_3^+$ based on the characteristic combinations of Zr, Cl, and F isotopes.

The $ZrFCl_3^+$ ion signal is the result of three F/Cl exchanges between $SiCl_4$ and ZrF_4. The observation of $ZrFCl_3^+$ indicates that complete F/Cl exchange to $ZrCl_4$ is not necessary for volatile release of a Zr-containing species. The QMS analysis also observed smaller ion signals for $ZrCl_4^+$ resulting from four F/Cl exchanges and $ZrF_2Cl_2^+$ resulting from two F/Cl

https://doi.org/10.1021/acs.chemmater.2c01603
Chem. Mater. 2022, 34, 8641−8653

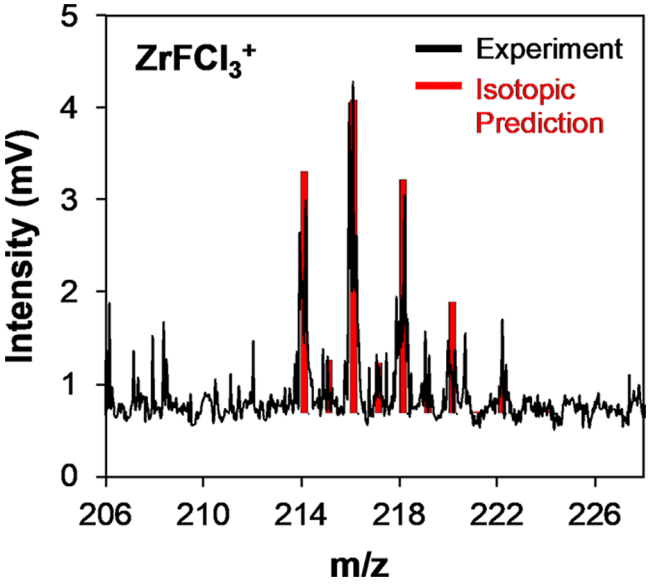

Figure 6. Mass spectrum showing ion intensities of $ZrFCl_3^+$ during the ligand-exchange reaction between $SiCl_4$ and ZrF_4 powder at 450 °C.

exchanges. The full mass spectrum from m/z 80−230 is given in Figure S3 in the Supporting Information.

The temperature dependence of the reaction between $SiCl_4$ and ZrF_4 powder is displayed in Figure 7. The reciprocal

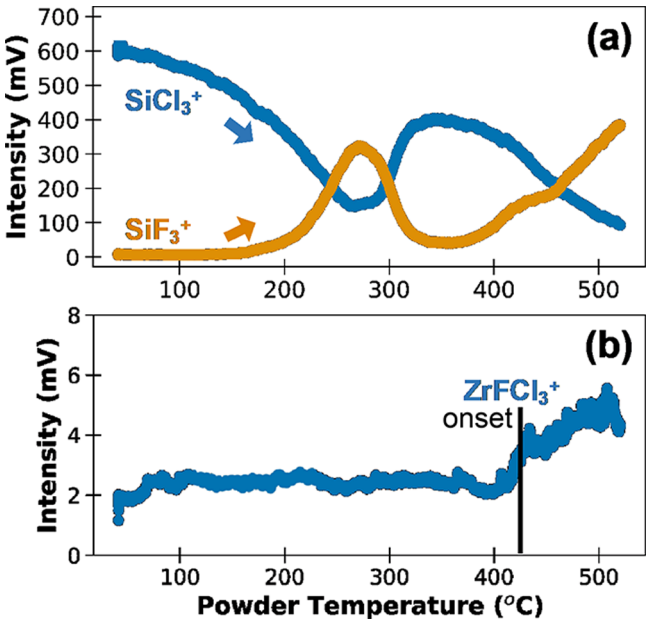

Figure 7. Ion intensities versus powder temperature during the reaction between $SiCl_4$ and ZrF_4 powder. (a) $SiCl_4$ precursor ($SiCl_3^+$) and SiF_4 ligand-exchange product (SiF_3^+) after total F/Cl exchange. (b) $ZrFCl_3$ metal etch product ($ZrFCl_3^+$).

relationship between the $SiCl_3^+$ and SiF_3^+ ion intensities is shown in Figure 7a. The ion intensity for $SiCl_3^+$ decreases as the ion intensity of SiF_3^+ increases from 175 to 275 °C. The ion intensity for $SiCl_3^+$ then increases as the ion intensity of SiF_3^+ decreases from 275 to 350 °C. Lastly, the ion intensity for $SiCl_3^+$ decreases as the ion intensity of SiF_3^+ increases from 350 to 530 °C. This complementary behavior argues for full F/Cl exchange for $SiCl_4$ in its reaction with ZrF_4 powder throughout the entire temperature range.

The correlated increases and decreases in the ion intensities for $SiCl_3^+$ and SiF_3^+ in Figure 7a can be interpreted in terms of the buildup of chlorine on the ZrF_4 powder. As the chlorine coverage increases on the metal fluoride surface, less fluorine species are available for ligand exchange. This chlorine buildup could explain the decrease of the SiF_3^+ ligand-exchange product from 275 to 350 °C. The $ZrFCl_3$ metal chloride etch products then are desorbed at >400 °C as shown in Figure 7b. As chlorine is lost from the metal fluoride powder, more fluorine surface species are available and ligand exchange can again convert the $SiCl_4$ precursor to the SiF_4 ligand-exchange product.

The onset temperature for F/Cl exchange as measured by the appearance of the SiF_3^+ ion signal in Figure 7a is 175 °C. In contrast, Figure 7b shows that the ion intensity for $ZrFCl_3^+$, from the main metal etch product, was not observed until 425 °C. $ZrCl_4$ can be used as a proxy for $ZrFCl_3$. $ZrCl_4$ exhibits a high vapor pressure of 0.51 Torr at 175 °C and 1240 Torr at 350 °C.[34] Therefore, $ZrFCl_3$ is expected to desorb if $ZrFCl_3$ is formed at the onset for ligand exchange at 175 °C. The expected $ZrFCl_3$ vapor pressure cannot explain the large temperature difference between the appearance of ligand-exchange products and metal etching products.

The measured $ZrFCl_3^+$ ion signals were also low. SiF_3^+ ion signals were measured with intensities as high as 400 mV in Figure 6a. In contrast, the $ZrFCl_3^+$ ion signals observed in Figure 6b were only around 1% of the SiF_3^+ ion signals in Figure 7a. The low signals of the Zr-containing etch products may result from lower ionization cross sections. In addition, the low signals could be due to a dilution effect. As F/Cl exchange occurs between the $SiCl_4$ precursor and the ZrF_4 surface, the Cl ligands initially exchanged with ZrF_4 on the surface could be diluted in the underlying ZrF_4 powder. Because of this dilution, volatile $ZrF_xCl_y^+$ species may not be detected until higher temperatures after enough Cl has built up in the ZrF_4 powder.

3.1.D. InF_3, HfF_4, and SnF_4. Similar experiments were conducted using InF_3, HfF_4, and SnF_4 powders. The temperature dependence of the reaction of $SiCl_4$ with InF_3 and HfF_4 powder was reported earlier.[16] The temperature dependence of the reaction of $SiCl_4$ with SnF_4 powder is presented in the Supporting Information in Figure S4.

3.2. Heteroleptic $SiCl_2(CH_3)_2$ Precursor with Cl and CH_3 Ligands. $SiCl_2(CH_3)_2$ (dichlorodimethyl-silane) is a heteroleptic silane precursor that contains both Cl and CH_3 ligands. $SiCl_2(CH_3)_2$ can be employed to determine the relative rates between F/Cl and F/CH_3 ligand exchange. $SiCl_2(CH_3)_2$ has not been used as a ligand-exchange precursor for thermal ALE.

3.2.A. GaF_3. The reaction of $SiCl_2(CH_3)_2$ with GaF_3 powder resulted in the observation of $GaCl_2^+$ and $GaCl_3^+$ ion signals as the metal etch products, similar to the reaction of $SiCl_4$ with GaF_3 powder displayed in Figure 2. These Cl-containing metal etch products indicate that F/Cl ligand exchange dominates over F/CH_3 ligand exchange. Temperature-dependent results for the reaction between $SiCl_2(CH_3)_2$ and GaF_3 powder are presented in Figure 8.

Figure 8a shows the ion signals for $SiCl_2(CH_3)^+$, the main ion signal from the $SiCl_2(CH_3)_2$ precursor, and $SiF_2(CH_3)^+$, the main ion signal from the $SiF_2(CH_3)_2$ ligand-exchange product.[35] The decreases and increases of the $SiCl_2(CH_3)^+$ and

https://doi.org/10.1021/acs.chemmater.2c01603
Chem. Mater. 2022, 34, 8641−8653

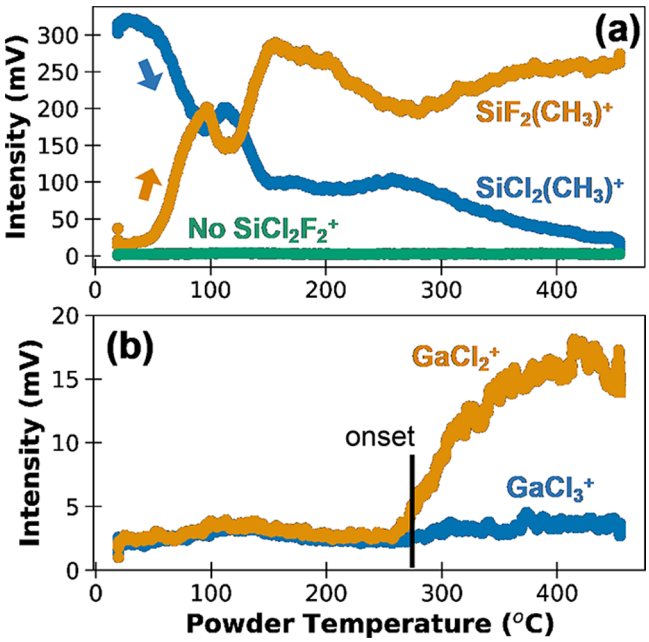

Figure 8. Ion intensities versus powder temperature during the reaction between $SiCl_2(CH_3)_2$ and GaF_3 powder. (a) $SiCl_2(CH_3)_2$ precursor ($SiCl_2(CH_3)^+$), $SiF_2(CH_3)_2$ ligand-exchange product ($SiF_2(CH_3)^+$), and possible $SiCl_2F_2$ ligand-exchange product after complete F/CH_3 exchange ($SiCl_2F_2^+$). (b) $GaCl_3$ metal etch product ($GaCl_3^+$) and its fragment $GaCl_2^+$.

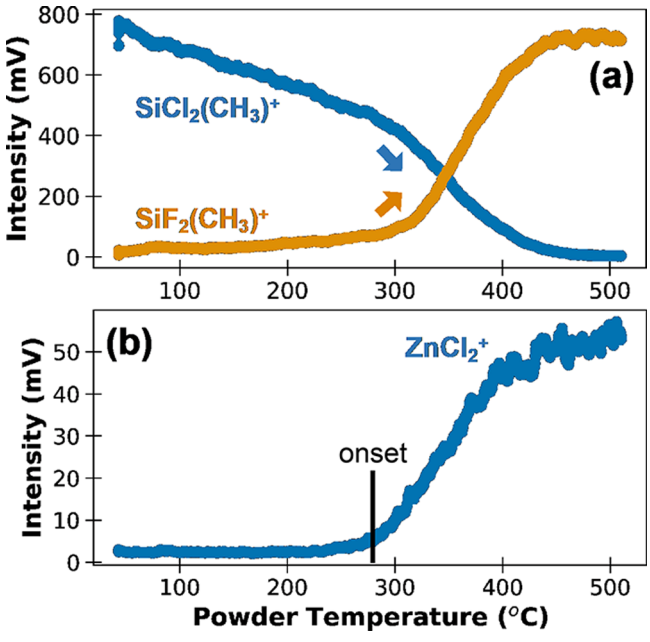

Figure 9. Ion intensities versus powder temperature during the reaction between $SiCl_2(CH_3)_2$ and ZnF_2 powder. (a) $SiCl_2(CH_3)_2$ precursor ($SiCl_2(CH_3)^+$) and $SiF_2(CH_3)_2$ ligand-exchange product after total F/Cl exchange ($SiF_2(CH_3)^+$). (b) $ZnCl_2$ metal etch product ($ZnCl_2^+$).

$SiF_2(CH_3)^+$ ion signals are correlated with each other. This complementary behavior argues that complete F/Cl ligand exchange is the dominant ligand-exchange reaction throughout the temperature ramp. The complementary behavior may be partially explained by the buildup of chlorine on the GaF_3 surface. When the $GaCl_3$ desorbs at >275 °C, more fluorine species are available for ligand exchange and the $SiF_2(CH_3)^+$ ion signal increases and the $SiCl_2(CH_3)^+$ ion signal decreases.

There is no evidence for any F/CH_3 ligand exchange from the ligand-exchange products. For example, the baseline intensity of $SiCl_2F_2^+$ in Figure 8a demonstrates the lack of products from total F/CH_3 exchange. Furthermore, products indicative of partial F/CH_3 exchange were also not observed such as $SiCl_2(CH_3)F^+$ and its possible fragments. $Ga(CH_3)_3$ and its fragments were also not produced resulting from the lack of F/CH_3 exchange.

The ion signals for the metal etch products are displayed in Figure 8b. These ion intensities are consistent with the electron impact ionization of $GaCl_3$.[28] The results for the $GaCl_2^+$ and $GaCl_3^+$ ion intensities are also very similar in Figure 8b and Figure 3c. This similarity between $SiCl_2(CH_3)_2$ in Figure 8b and $SiCl_4$ in Figure 3c argues that F/Cl is the main ligand-exchange reaction.

3.2.B. ZnF_2. The reaction between $SiCl_2(CH_3)_2$ and ZnF_2 powder produced $ZnCl_2^+$ ion signals from the $ZnCl_2$ metal etch product similar to the reaction of $SiCl_4$ with ZnF_2 powder displayed in Figure 4. These Cl-containing metal etch products again indicate that F/Cl exchange is dominant. Figure 9a shows the temperature dependence of the reaction between $SiCl_2(CH_3)_3$ and ZnF_2. The correlation between the decrease in the $SiCl_2(CH_3)^+$ ion signal for the precursor and the increase in the $SiF_2(CH_3)^+$ ion signal for the ligand-exchange product in Figure 9a is very complementary and consistent with total F/Cl exchange over the entire temperature ramp. There is no evidence for any F/CH_3 exchange. The QMS measurements did monitor minor $SiFCl(CH_3)_2^+$ ion signals that arise from partial F/Cl exchange. However, these ion signals have intensities < 80 mV and are not shown in Figure 9a.

Figure 9b shows $ZnCl_2$, the dominant metal etch product. No ion signals were observed that were consistent with $Zn(CH_3)_2^+$, $ZnF(CH_3)^+$, or any of their possible fragments. The $ZnCl_2^+$ ion signal was observed with an onset etching temperature of 280 °C. This onset temperature is similar to the onset temperature of 250 °C for the $SiF_2(CH_3)^+$ ion signal resulting from full F/Cl exchange for $SiCl_2(CH_3)_2$ in its reaction with ZnF_2 powder. $ZnCl_2$ can desorb nearly as soon as $ZnCl_2$ is formed by ligand exchange.

3.2.C. ZrF_4. The reaction between $SiCl_2(CH_3)_2$ and ZrF_4 powder produced $ZrFCl_3^+$ ion signals from the $ZrFCl_3$ metal etch product similar to the reaction of $SiCl_4$ with ZrF_4 powder displayed in Figure 6. These results again support F/Cl ligand exchange as the sole ligand-exchange reaction. Temperature-dependent results for the reaction between $SiCl_2(CH_3)_2$ and ZrF_4 powder are shown in Figure 10. As expected if F/Cl exchange is the only ligand-exchange reaction, the $SiCl_2(CH_3)^+$ and $SiF_2(CH_3)^+$ ion intensities are highly correlated in Figure 10a. The complementary behavior may be partially explained by the buildup and desorption of chlorine on the ZrF_4 surface.

The F/Cl exchange was observed with an onset temperature at 140 °C as displayed in Figure 10a. However, the $ZrCl_4^+$ and $ZrFCl_3^+$ ion intensities from the Zr-containing etch products were not observed until 375 °C as shown in Figure 10b. The large difference in the onset temperatures for ligand-exchange and metal etch products again suggests that Cl needs to build up in the ZrF_4 powder before $ZrCl_4$ can desorb as a metal etch product. In addition, the large ion signal intensity differences between $SiF_2(CH_3)^+$ and $ZrFCl_3^+$ or $ZrCl_4^+$ suggests that either the Zr-containing etch products have lower ionization

https://doi.org/10.1021/acs.chemmater.2c01603
Chem. Mater. 2022, 34, 8641−8653

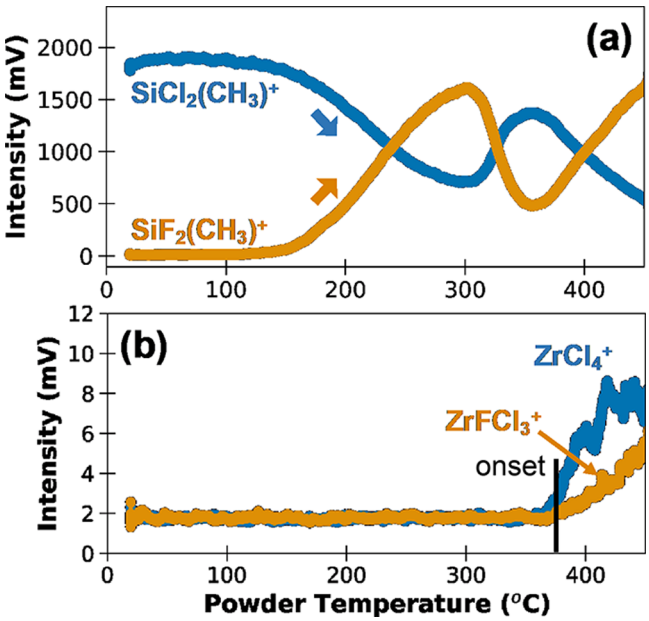

Figure 10. Ion intensities versus powder temperature during the reaction between $SiCl_2(CH_3)_2$ and ZrF_4 powder. (a) $SiCl_2(CH_3)_2$ precursor ($SiCl_2(CH_3)^+$) and $SiF_2(CH_3)_2$ ligand-exchange product after total F/Cl exchange ($SiF_2(CH_3)^+$). (b) $ZrCl_4$ and $ZrFCl_3$ metal etch products ($ZrCl_4^+$ and $ZrFCl_3^+$).

cross sections or that the Cl ligands may be diluted in the ZrF_4 powder.

There was no evidence for F/CH_3 exchange in the ligand-exchange products for the reaction between $SiCl_2(CH_3)_2$ and ZrF_4 powder. The lack of F/CH_3 exchange is consistent with a small Zr−CH_3 bond energy and the low decomposition temperature of ≤15 °C for $Zr(CH_3)_4$.[36] The weak Zr-CH_3 bond also explained the lack of thermal ZrO_2 ALE using HF and $Al(CH_3)_3$ as the reactants.[8,37]

3.3. Heteroleptic $SiCl(CH_3)_2H$ Precursor with Cl, CH_3, and H Ligands. $SiCl(CH_3)_2H$ (chlorodimethyl-silane) is a heteroleptic precursor. The ligand exchange between $SiCl(CH_3)_2H$ with metal fluorides could occur with F/Cl, F/CH_3 or F/H exchange. $SiCl(CH_3)_2H$ has not been used as a ligand-exchange precursor for thermal ALE.

3.3.A. GaF_3. The reaction between $SiCl(CH_3)_2H$ and GaF_3 powder produced $GaCl_2^+$ and $GaCl_3^+$ ion signals similar to the reaction of $SiCl_4$ with GaF_3 powder displayed in Figure 2. Even though CH_3 and H ligands could participate, the Cl-containing metal etch products indicate that F/Cl ligand exchange is dominant. Figure 11a shows the temperature dependence of the reaction between $SiCl(CH_3)_2H$ and GaF_3 powder. Below 200 °C, there is correlated behavior between the $SiCl(CH_3)_2^+$ ion intensity for the precursor and the $SiF(CH_3)_2^+$ ion intensity for the main ligand-exchange product.[35] The $SiF(CH_3)_2^+$ ion intensity at a m/z value of 93 is attributed to the ionization of $SiF(CH_3)_2H$.[35] This complementary behavior argues for dominant F/Cl exchange between $SiCl(CH_3)_2H$ and the GaF_3 powder. In addition, the F/Cl exchange has a low onset temperature of 60 °C.

Figure 11b shows the ion intensities for the species that result from F/H exchange. The $SiF_2(CH_3)_2^+$ ion intensity indicates both F/H and F/Cl exchange. The $SiCl(CH_3)F^+$ ion intensity indicates only F/H exchange. However, the $SiF_2(CH_3)_2^+$ and $SiCl(CH_3)F^+$ ion intensities are much lower than the ion intensity for $SiF(CH_3)_2^+$ in Figure 11a.

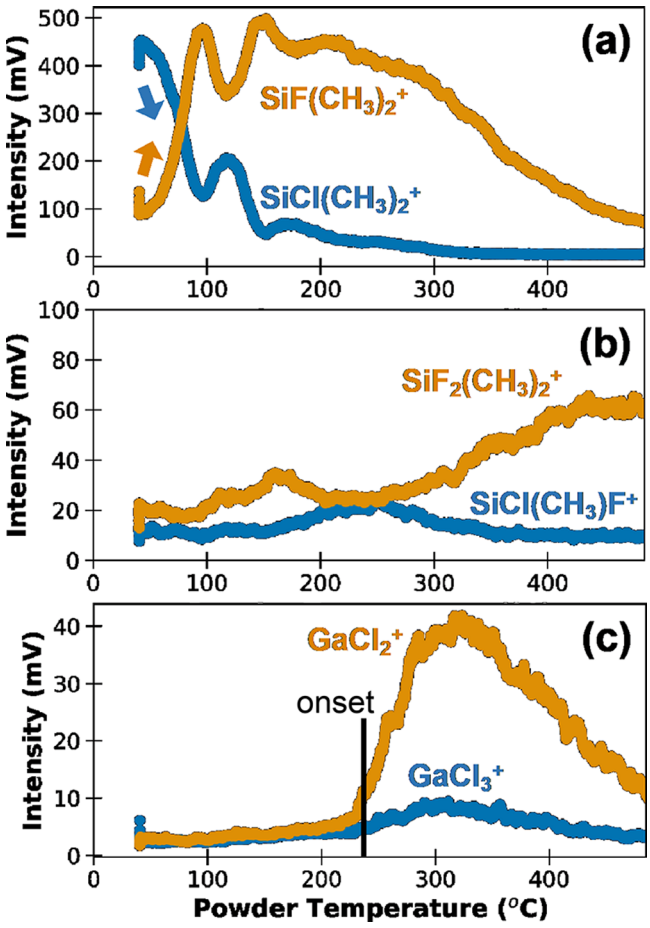

Figure 11. Ion intensities versus powder temperature during the reaction between $SiCl(CH_3)_2H$ and GaF_3 powder. (a) $SiCl(CH_3)_2H$ precursor ($SiCl(CH_3)_2^+$) and $SiF(CH_3)_2H$ ligand-exchange product after F/Cl exchange ($SiF(CH_3)_2^+$). (b) $SiCl(CH_3)_2F$ ligand-exchange product after F/H exchange ($SiCl(CH_3)_2F^+$) and $SiF_2(CH_3)_2$ ligand-exchange product after both F/Cl and F/H exchange ($SiF_2(CH_3)_2^+$). (c) $GaCl_3$ metal etch product ($GaCl_3^+$) and its fragment $GaCl_2^+$.

The onset temperature for the $SiF_2(CH_3)_2^+$ ion intensity resulting from both F/H and F/Cl exchange is observed at 350 °C. This onset temperature is much higher than the onset temperature of 60 °C for the $SiF(CH_3)_2^+$ ion intensity resulting from F/Cl exchange.

Figure 11c shows that the $GaCl_3^+$ ion intensity for the metal etch product has an onset temperature of 240 °C. This onset temperature is much higher than the onset temperature of 60 °C for F/Cl exchange in Figure 11a. This difference again argues that Cl must be building up in the GaF_3 powder prior to the desorption of $GaCl_3$ at 240 °C. There is also a similarity between the onset temperatures for the observation of $GaCl_2^+$ and $GaCl_3^+$ ion intensities during the reaction of $SiCl_4$, $SiCl_2(CH_3)_2$ and $SiCl(CH_3)_2H$ with GaF_3 powder in Figures 3c, 8b and 11c. Independent of the exact nature of the silane, the presence of Cl ligands and F/Cl exchange are the most important factors for the ligand-exchange reaction.

3.3.B. ZnF_2. For the reaction of the heteroleptic $SiCl(CH_3)_2H$ precursor with ZnF_2 powder, $ZnCl_2^+$ ion signals were detected as the metal etch products similar to the reaction of $SiCl_4$ with ZnF_2 powder shown in Figure 4. The Cl-containing metal etch products indicate that F/Cl ligand exchange is dominant. Figure 12a shows the temperature dependence of

https://doi.org/10.1021/acs.chemmater.2c01603
Chem. Mater. 2022, 34, 8641−8653

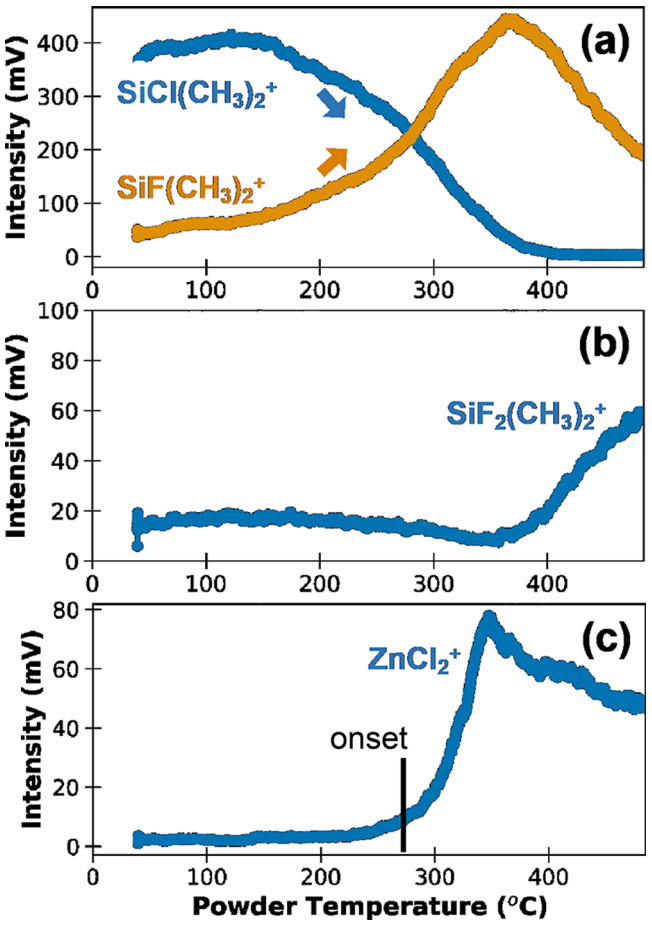

Figure 12. Ion intensities versus powder temperature during the reaction between $SiCl(CH_3)_2H$ and ZnF_2 powder. (a) $SiCl(CH_3)_2H$ precursor ($SiCl(CH_3)_2^+$) and $SiF(CH_3)_2H$ ligand-exchange product after F/Cl exchange ($SiF(CH_3)_2^+$). (b) $SiF_2(CH_3)_2$ ligand-exchange product after both F/Cl and F/H exchange $(SiF_2(CH_3)_2)^+$. (c) $ZnCl_2$ metal etch product ($ZnCl_2^+$).

the reaction between $SiCl(CH_3)_2H$ and ZnF_2 powder. The $SiCl(CH_3)_2^+$ ion intensity decreases in conjunction with the increase in the $SiF(CH_3)_2^+$ ion intensity. This ligand-exchange product results from F/Cl exchange as expected from the observation of $ZnCl_2^+$ as the metal etch product. The onset temperature for the $SiF(CH_3)_2^+$ ion intensity is 180 °C.

The complementary behavior between the $SiCl(CH_3)_2^+$ and $SiF(CH_3)_2^+$ ion intensities is lost at >370 °C when the $SiF(CH_3)_2^+$ ion intensity decreases with no corresponding rise in the $SiCl(CH_3)_2^+$ ion intensity. This change results from the rise of the $SiF_2(CH_3)_2^+$ ion intensity shown in Figure 12b. The $SiF_2(CH_3)_2^+$ ion intensity results from both F/Cl and F/H exchange between $SiCl(CH_3)_2H$ and the ZnF_2 powder. This observation indicates that F/H exchange becomes competitive with F/Cl exchange at higher temperatures.

Figure 12c shows that $ZnCl_2$ is observed as the main metal etch product. The $ZnCl_2^+$ ion signals have an onset temperature at 275 °C. This onset temperature is higher than the onset temperature for F/Cl exchange at 180 °C. The Cl ligands are building up prior to the desorption of $ZnCl_2$ at ≥275 °C. In addition, there is a similarity between the onset temperatures for the $ZnCl_2^+$ ion intensity for the reaction of $SiCl_4$, $SiCl_2(CH_3)_2$ and $SiCl(CH_3)_2H$ with ZnF_2 powder in Figures 5b, 9b, and 12c. This behavior again demonstrates that F/Cl exchange is the dominant ligand-exchange pathway for all the silane precursors.

3.3.C. ZrF_4. For the reaction of $SiCl(CH_3)_2H$ with ZrF_4 powder, $ZrFCl_3^+$ ion signals were detected as the metal etch products similar to the reaction of $SiCl_4$ with ZrF_4 powder shown in Figure 6. The Cl-containing metal etch products argue that F/Cl ligand exchange is the dominant ligand-exchange pathway. Ligand exchange with CH_3 and H ligands is not occurring during the reaction of $SiCl(CH_3)_2H$ with ZrF_4 powder.

In support of F/Cl ligand exchange, Figure 13a shows remarkably complementary behavior between the $SiCl(CH_3)_2^+$

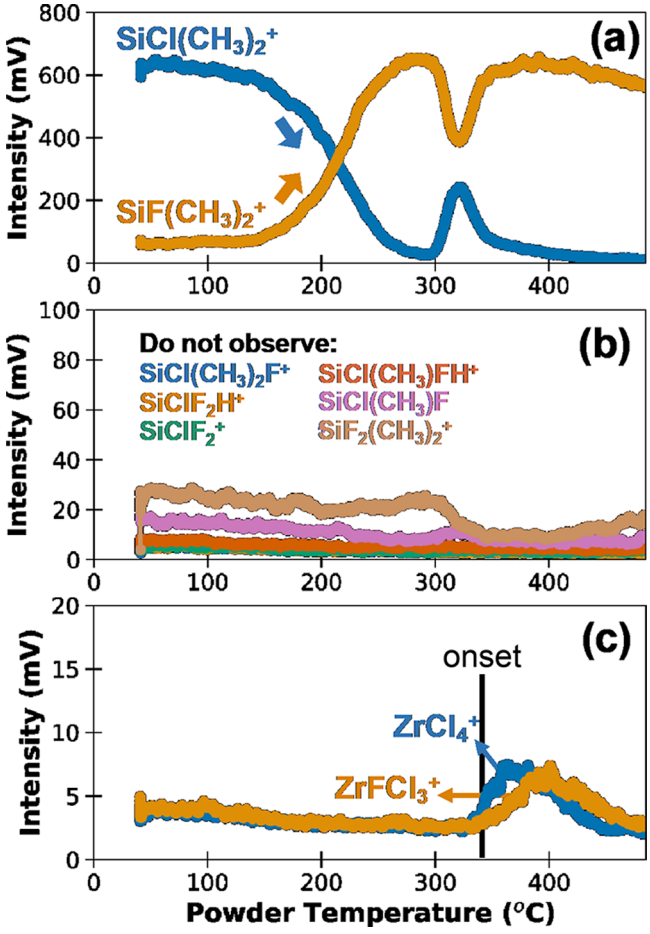

Figure 13. Ion intensities versus powder temperature during the reaction between $SiCl(CH_3)_2H$ and ZrF_4 powder. (a) $SiCl(CH_3)_2H$ precursor ($SiCl(CH_3)_2^+$) and $SiF(CH_3)_2H$ ligand-exchange product after F/Cl exchange ($SiF(CH_3)_2^+$). (b) $SiCl(CH_3)_2H$ precursor after F/CH_3 or F/H exchange (many possible species, not observed). (c) $ZrCl_4$ and $ZrFCl_3$ metal etch products ($ZrCl_4^+$ and $ZrFCl_3^+$).

ion intensity for the precursor and the $SiF(CH_3)_2^+$ ion intensity for the main ligand-exchange product. The $SiCl(CH_3)_2^+$ and $SiF(CH_3)_2^+$ ion intensities in Figure 13a form near mirror images of each other. The prominent decrease/increase of the $SiF(CH_3)_2^+/SiCl(CH_3)_2^+$ signals from 300 to 325 °C and the subsequent increase/decrease of the $SiF(CH_3)_2^+/SiCl(CH_3)_2^+$ signals from 325 to 350 °C correlate with the onset of $ZrFCl_3$ and $ZrCl_4$ desorption at 325 °C. The buildup of chlorine can decrease the ligand-exchange reaction. The loss of chlorine by metal chloride desorption can then increase the ligand-exchange reaction.

https://doi.org/10.1021/acs.chemmater.2c01603
Chem. Mater. 2022, 34, 8641−8653

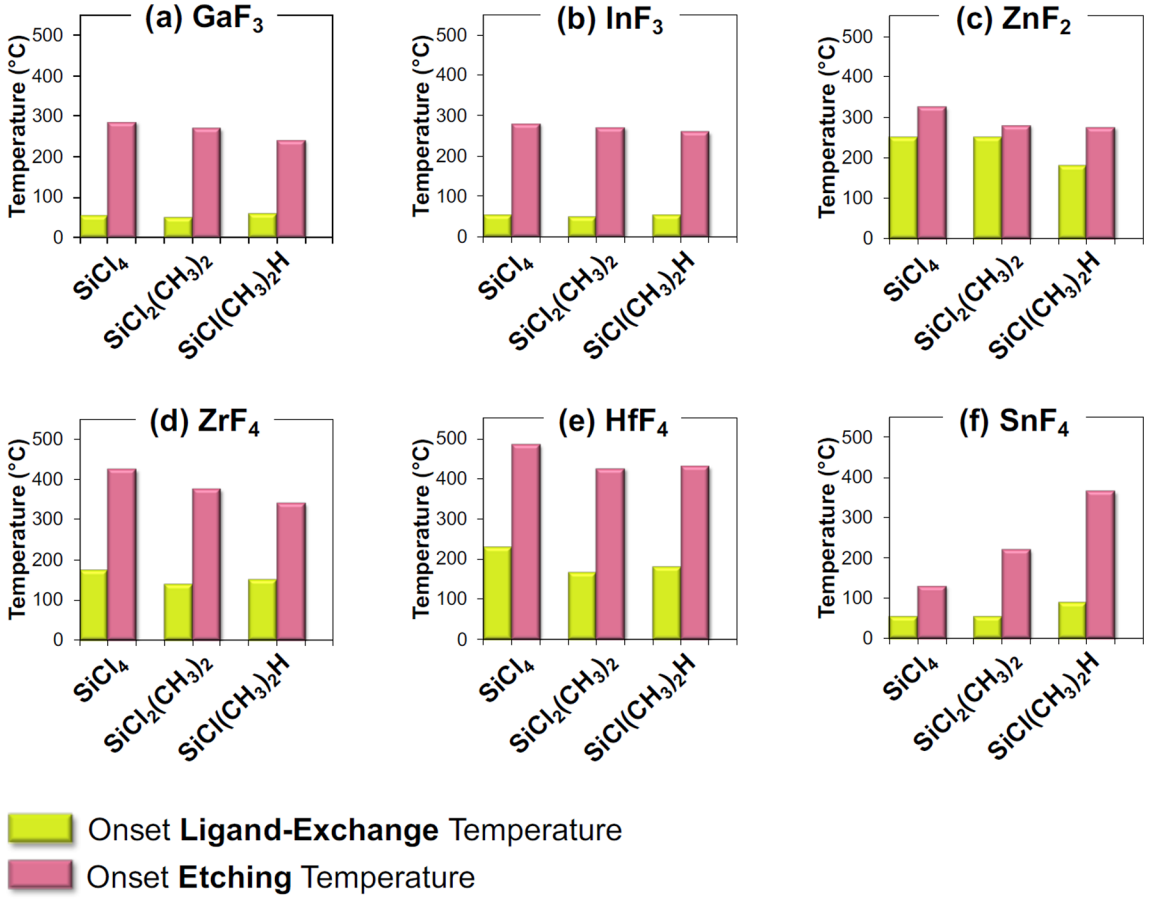

Figure 14. Onset temperatures for ligand exchange and metal etching observed for spontaneous etching of various metal fluorides (GaF_3, InF_3, ZnF_2, ZrF_4, HfF_4, and SnF_4) using different silane precursors ($SiCl_4$, $SiCl_2(CH_3)_2$, and $SiCl(CH_3)_2H$).

There are also no species observed from possible F/CH_3 or F/H exchange. All of the species that may result from F/CH_3 or F/H exchange are shown in Figure 13b. All of these species are negligible. Due to the dominant F/Cl exchange, the metal etch products produced $ZrF_xCl_y^+$ ion species as displayed in Figure 13c. The $ZrCl_4^+$ and $ZrFCl_3^+$ ion signals provide evidence for both complete and partial F/Cl exchange between the $SiCl(CH_3)_2H$ precursor and the ZrF_4 powder. The Zr-containing etch products have an onset temperature of 340 °C. This onset temperature is much higher than the onset temperature of 150 °C for F/Cl exchange. This temperature difference again indicates that Cl buildup in the ZrF_4 powder may be required for volatile release of the Zr-containing etch products.

The low intensities of the Zr-containing etch products observed in Figure 13c may result from low ionization efficiencies or a dilution effect as suggested earlier. There is also a similarity between the onset temperatures for the $ZrFCl_3^+$ and $ZrCl_4^+$ ion intensities for the reactions of $SiCl_4$, $SiCl_2(CH_3)_2$ and $SiCl(CH_3)_2H$ with ZrF_4 powder in Figures 7b, 10b and 13c. This similarity again argues that F/Cl exchange is the main ligand-exchange pathway.

3.4. Homoleptic $Si(CH_3)_4$ Precursor with Only CH_3 Ligands. $Si(CH_3)_4$ (tetramethyl-silane) is a homoleptic silane precursor that only contains CH_3 ligands. In the absence of Cl ligands, $Si(CH_3)_4$ can test if F/CH_3 exchange is possible when F/CH_3 exchange is the only option. In all cases, no ligand-exchange products or metal etch products were observed for the reaction of $Si(CH_3)_4$ with any of the metal fluorides. These experiments confirm that F/CH_3 exchange is not favorable even in the absence of Cl ligands.

3.5. Onset Temperatures for Ligand-Exchange and Etching Reactions. The onset temperatures for ligand-exchange and etching reactions for the various silane precursors with all the metal fluorides are shown in Figure 14. The onset temperatures for the various metal fluorides include GaF_3, ZnF_2 and ZrF_4 that have been discussed earlier in this paper. In addition, the onset temperatures are also given for InF_3, HfF_4 and SnF_4 that were examined using similar experiments. The differences between the metal fluorides reveal the diverse landscape for the spontaneous etching of metal fluorides by silane precursors using ligand-exchange reactions.[16] In some cases, the metal etch products can appear at much higher temperatures than the onset temperature for the ligand-exchange products. The metal etch products can also appear at temperatures that are comparable to the onset temperature for the ligand-exchange products.

GaF_3 in Figure 14a and InF_3 in Figure 14b display similar trends. Both GaF_3 and InF_3 are Group 13 metal fluorides. The onset temperatures for ligand exchange are comparable at 50−60 °C. The onset temperatures for metal etching are also comparable at 240−285 °C. Both GaF_3 and InF_3 have a large difference between their onset temperatures for ligand-exchange and metal etching reactions. The difference between the two onset temperatures is in the range of 180−230 °C.

Although GaF_3 and InF_3 display comparable behavior in Figure 14a,b, $GaCl_3$ and $InCl_3$ have different vapor pressures. $GaCl_3$ has a vapor pressure of 1 Torr at 48 °C.[31,38] $InCl_3$ does

https://doi.org/10.1021/acs.chemmater.2c01603
Chem. Mater. 2022, 34, 8641−8653

not obtain a vapor pressure of 1 Torr until ~350 °C.[39] $GaCl_3$ should have sufficient vapor pressure at ≥1 Torr to desorb at or above the onset temperatures for ligand exchange. In contrast, $InCl_3$ will have a much lower pressure at the onset temperature for ligand-exchange. $InCl_3$ desorption would not be anticipated until much higher temperatures.

Given that $GaCl_3$ and $InCl_3$ have very different vapor pressures, the similarity between parts a and b of Figure 14 must be explained by a different mechanism. The dilution of the Cl from F/Cl exchange in the metal fluoride could explain the large difference between the onset temperatures for ligand-exchange and metal etch products. Perhaps a critical concentration of Cl is required in the metal fluoride prior to desorption of the $GaCl_3$ or $InCl_3$ metal etch products.

ZnF_2 in Figure 14c demonstrates the case where the ligand exchange and metal etch products are observed at similar temperatures. The onset temperatures for ligand exchange at between 180 and 250 °C are noticeably higher than for the other metal fluorides. These higher onset temperatures may result from less favorable ligand-exchange reactions with ZnF_2. In comparison, the onset temperatures for metal etch products are between 275 and 325 °C. The resulting difference between the two onset temperatures is only 30−95 °C.

The $ZnCl_2$ metal etch product resulting from the F/Cl exchange has the lowest vapor pressure of all the various metal chloride etch products. $ZnCl_2$ has a vapor pressure of only 0.025 Torr at 300 °C[40] and 1 Torr at 428 °C.[38] The similar onset temperatures may indicate that the Cl from ligand exchange forms $ZnCl_2$ on the surface of the ZnF_2 powder. $ZnCl_2$ then desorbs only when the temperatures are sufficient to sublime $ZnCl_2$.

ZrF_4 and HfF_4 are Group 4 metal fluorides. ZrF_4 in Figure 14d and HfF_4 in Figure 14e both display a difference between the onset temperatures for ligand-exchange and metal etch products. The onset temperatures for ligand exchange are between 140 and 230 °C. The onset temperatures for metal etching are between 340 and 485 °C. The resulting difference between the two onset temperatures is in the range of 190−260 °C. $ZrCl_4$ and $HfCl_4$ both have similar vapor pressures at and above the onset temperatures for ligand exchange. $ZrCl_4$ has a vapor pressure of 1 Torr at 180 °C.[41] $HfCl_4$ has a vapor pressure of 1 Torr at 170 °C.[41] Similar onset temperatures for the metal etch products are expected if the products have comparable vapor pressures.

The trends for SnF_4 in Figure 14f are different than the other metal fluorides. For SnF_4, the onset temperatures for metal etch products exhibit a dependence on the number of Cl ligands in the silane precursor. The reaction of $SiCl_4$ with SnF_4 displays an onset temperature for metal etch products at 130 °C. The reaction of $SiCl_2(CH_3)_2$ with SnF_4 displays a higher onset temperature for metal etch products at 220 °C. The reaction of $SiCl(CH_3)_2H$ with SnF_4 has an even higher onset temperature for metal etch products at 365 °C. In all cases, F/Cl exchange is the ligand-exchange pathway and $SnCl_4$ is the exclusive metal etch product.

The very high volatility of $SnCl_4$ may explain the dependence between the onset temperature for metal etch products and the number of Cl ligands in the silane precursor in Figure 14f. The vapor pressure of $SnCl_4$ is 26 Torr at room temperature.[42] With such a high $SnCl_4$ volatility, $SnCl_4$ can desorb as a metal etch product as soon as there is sufficient F/Cl exchange between the silane precursor and the SnF_4 powder. Although the SnF_4 onset temperatures scale inversely with the number of Cl ligands in the silicon precursor in Figure 14f, a longer exposure time with a silane with fewer Cl ligands may be expected to display a lower onset temperature. Future experiments at different heating rates should be conducted to test this proposition.

3.6. Thermochemical Calculations of Ligand-Exchange Reactions. Successful thermal ALE requires favorable thermodynamics for the modification and volatile release reactions. The favorability of the ligand-exchange reaction can be measured by the change in Gibbs free energy (ΔG). Figure 15 shows the ΔG values for the ligand-exchange reaction between $SiCl_4$ and GaF_3, ZnF_2, and ZrF_4 at 350 °C. The ligand exchange is examined for all the possible F/Cl exchanges between the $SiCl_4$ precursor and the metal fluoride. Figure 15 shows that GaF_3, ZnF_2, and ZrF_4 all exhibit negative ΔG values for ligand exchange with $SiCl_4$. These negative ΔG values support the QMS observation of metal chlorides as the metal etch products using $SiCl_4$ as the precursor for ligand exchange.

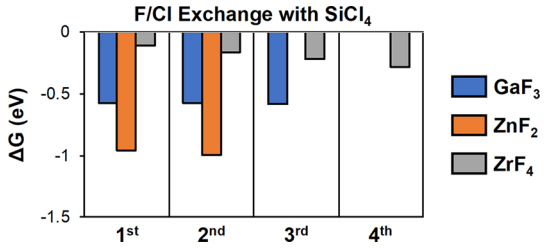

Figure 15. Thermochemical calculations for change in Gibbs free energy (ΔG) at 350 °C for sequential F/Cl exchange between $SiCl_4$ with GaF_3, ZnF_2, and ZrF_4.

Figure 16 displays the ΔG values for ligand exchange between $SiCl_2(CH_3)_2$ and GaF_3, ZnF_2, and ZrF_4 at 350 °C. For the F/Cl exchange in Figure 16a, the ΔG values are negative for all three metal fluorides. The ΔG values are also similar to the ΔG values for $SiCl_4$ in Figure 15. The total F/Cl exchange

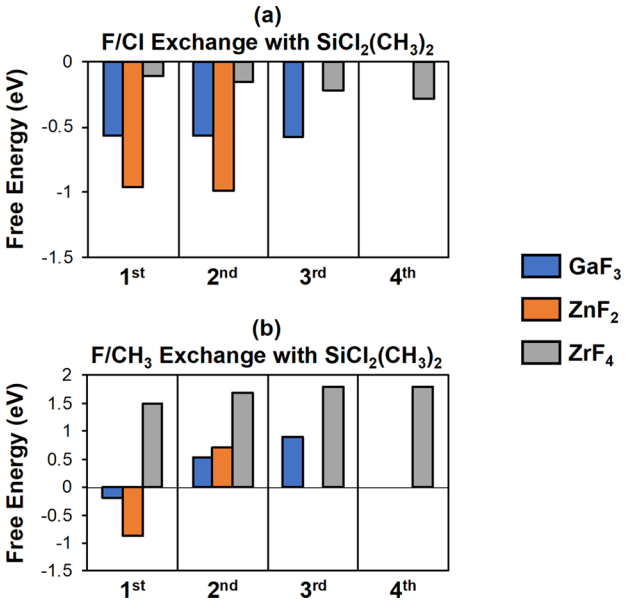

Figure 16. Thermochemical calculations of change in Gibbs free energy (ΔG) at 350 °C for sequential (a) F/Cl exchange and (b) F/CH_3 exchange between $SiCl_2(CH_3)_2$ with GaF_3, ZnF_2, and ZrF_4.

https://doi.org/10.1021/acs.chemmater.2c01603
Chem. Mater. 2022, 34, 8641−8653

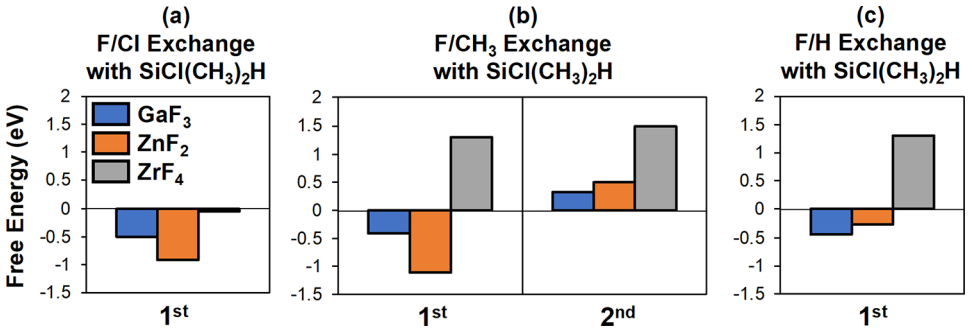

Figure 17. Thermochemical calculations of change in Gibbs free energy (ΔG) at 350 °C for sequential (a) F/Cl exchange, (b) F/CH_3 exchange, and (c) F/H exchange between $SiCl(CH_3)_2H$ with GaF_3, ZnF_2, and ZrF_4.

between $SiCl_2(CH_3)_2$ and the three metal fluorides is thermochemically favorable. These results support the observation of metal chlorides as metal etch products.

In contrast, Figure 16b reveals that the F/CH_3 exchange is only favorable for the first F/CH_3 exchange with GaF_3 and ZnF_2. The subsequent F/CH_3 exchanges have positive ΔG values for all the metal fluorides. For F/CH_3 exchange with ZrF_4, none of the F/CH_3 exchanges are favorable. These results agree with the lack of any observed methylated metal etch products during the QMS experiments.

Figure 17 shows the ΔG values for ligand exchange between $SiCl(CH_3)_2H$ and GaF_3, ZnF_2, and ZrF_4 at 350 °C. Figure 17a indicates that F/Cl exchange is thermochemically favorable for all three metal fluorides. These results are consistent with the observation of metal chlorides as the metal etch products when using $SiCl(CH_3)_2H$ as the ligand-exchange precursor. In addition, Figure 17b reveals that F/CH_3 exchange is favorable with GaF_3 and ZnF_2 only for the first F/CH_3 exchange. The second F/CH_3 exchange is thermochemically unfavorable. These results support the absence of any methylated metal etch products observed as volatile etch products during the QMS experiments.

Lastly, Figure 17c shows that F/H exchange has negative ΔG values and is favorable only between $SiCl(CH_3)_2H$ and GaF_3 or ZnF_2. These negative ΔG values are consistent with the observation of F/H exchange for the reaction of $SiCl(CH_3)_2H$ with GaF_3 in Figure 11b and with ZnF_2 in Figure 12b. The positive ΔG for the reaction of $SiCl(CH_3)_2H$ with ZrF_4 in Figure 17c is also in agreement with the lack of any F/H exchange between $SiCl(CH_3)_2$ with ZrF_4 in Figure 13b.

The thermochemical calculations for the ligand-exchange reactions agree well with the QMS observations. The calculations determined that F/Cl exchange is favorable between all the Cl-containing silane precursors and the various metal fluorides. These results are consistent with metal chlorides as the dominant metal etch product.

4. CONCLUSIONS

The spontaneous etching of various metal fluorides with silane precursors containing different ligands was examined using *in situ* QMS investigations. The metal fluorides were GaF_3, InF_3, ZnF_2, ZrF_4, HfF_4, and SnF_4. The silane precursors for ligand exchange were $SiCl_4$, $SiCl_2(CH_3)_2$, $SiCl(CH_3)_2H$, and $Si(CH_3)_4$. These homoleptic and heteroleptic silane precursors provided an evaluation of the effectiveness of F/Cl, F/CH_3, and F/H ligand exchange with the metal fluorides. Even though all the different ligands could participate in the ligand-exchange reaction, the QMS studies revealed that F/Cl exchange was the dominant mechanism for ligand exchange. In addition, the metal chlorides $GaCl_3$, $InCl_3$, $ZnCl_2$, $ZrCl_4$, $HfCl_4$, and $SnCl_4$ were the only metal etch products resulting from the ligand-exchange reactions.

The QMS studies performed versus temperature revealed complementary behavior between the silane precursors and the silane products after the ligand-exchange reaction. During the temperature ramps, decreases/increases in the silane precursor were correlated with increases/decreases in the silane ligand-exchange product. This strong correspondence argued that there was one main ligand-exchange mechanism and the dominant pathway was F/Cl exchange. Many of the correlations were also consistent with chlorine buildup that lowers the available fluorine species and reduces the ligand-exchange reaction. Subsequently, metal chloride desorption exposes more fluorine species and increases the ligand-exchange reaction. For a given metal fluoride, the onset temperatures for the silane ligand-exchange products were similar for all the various silane precursors. Likewise, except for SnF_4, the onset temperatures for the metal chloride etch products from a given metal fluoride were similar for all the silane precursors.

The onset temperatures for the silane ligand-exchange products were always lower than the onset temperatures for the metal chloride etch products. The differences between the onset temperatures varied between the metal fluorides. The difference was the largest for GaF_3 and InF_3, the Group 13 metal fluorides, and ZrF_4 and HfF_4, the Group 4 metal fluorides. This large difference was attributed to the dilution of Cl and the slow buildup of Cl in the metal fluoride before the metal chlorides can form and volatilize. In contrast, the difference was small for ZnF_2. This small difference may be related to the less favorable ligand-exchange reactions and higher onset temperatures for ligand exchange with ZnF_2.

Thermochemical calculations were also consistent with the experimental observations. ΔG calculations for F/Cl exchange yielded the most negative ΔG values compared with F/CH_3 or F/H exchange. These results support the observation of metal chlorides as the metal etch products. In contrast, F/CH_3 exchange was either not favorable or could not occur more than once with a given metal fluoride. These results support the observation that metal methyl complexes do not form as volatile metal etch products. In addition, F/H exchange is predicted for the reaction of $SiCl(CH_3)_2H$ with GaF_3 and ZnF_2 in agreement with the experimental observations. The experimental and theoretical results are all consistent with

https://doi.org/10.1021/acs.chemmater.2c01603
Chem. Mater. 2022, 34, 8641−8653

dominant F/Cl exchange and metal chlorides as the volatile metal etch products.

■ ASSOCIATED CONTENT

Supporting Information

The Supporting Information is available free of charge at https://pubs.acs.org/doi/10.1021/acs.chemmater.2c01603.

Quadrupole mass spectrometry (QMS) results for $SiCl_4$ with GaF_3, ZnF_2, and ZrF_4 powder and temperature dependent QMS results for $SiCl_4$ with SnF_4 powder (PDF)

■ AUTHOR INFORMATION

Corresponding Author

Steven M. George − *Department of Chemistry, University of Colorado, Boulder, Colorado 80309, United States;* orcid.org/0000-0003-0253-9184; Email: steven.george@colorado.edu

Authors

Ann Lii-Rosales − *Department of Chemistry, University of Colorado, Boulder, Colorado 80309, United States*

Virginia L. Johnson − *Department of Chemistry, University of Colorado, Boulder, Colorado 80309, United States*

Andrew S. Cavanagh − *Department of Chemistry, University of Colorado, Boulder, Colorado 80309, United States;* orcid.org/0000-0002-6201-530X

Andreas Fischer − *Lam Research Corporation, Fremont, California 94538, United States*

Thorsten Lill − *Lam Research Corporation, Fremont, California 94538, United States*

Sandeep Sharma − *Department of Chemistry, University of Colorado, Boulder, Colorado 80309, United States;* orcid.org/0000-0002-6598-8887

Complete contact information is available at: https://pubs.acs.org/10.1021/acs.chemmater.2c01603

Notes

The authors declare no competing financial interest.

■ ACKNOWLEDGMENTS

This research was funded by the Lam Research Corporation. S.S. was supported through the National Science Foundation Grant CHE-2145209.

■ REFERENCES

(1) Fischer, A.; Routzahn, A.; George, S. M.; Lill, T. Thermal Atomic Layer Etching: A Review. *J. Vac. Sci. Technol. A* **2021**, *39*, 030801.

(2) George, S. M. Mechanisms of Thermal Atomic Layer Etching. *Acc. Chem. Res.* **2020**, *53*, 1151−1160.

(3) Lee, Y.; George, S. M. Atomic Layer Etching of Al_2O_3 Using Sequential, Self-Limiting Thermal Reactions with $Sn(acac)_2$ and Hydrogen Fluoride. *ACS Nano* **2015**, *9*, 2061−2070.

(4) Cano, A. M.; Marquardt, A. E.; DuMont, J. W.; George, S. M. Effect of HF Pressure on Thermal Al_2O_3 Atomic Layer Etch Rates and Al_2O_3 Fluorination. *J. Phys. Chem. C* **2019**, *123*, 10346−10355.

(5) Lee, Y.; DuMont, J. W.; George, S. M. Trimethylaluminum as the Metal Precursor for the Atomic Layer Etching of Al_2O_3 Using Sequential, Self-Limiting Thermal Reactions. *Chem. Mater.* **2016**, *28*, 2994−3003.

(6) Lee, Y.; George, S. M. Thermal Atomic Layer Etching of HfO_2 Using HF for Fluorination and $TiCl_4$ for Ligand-Exchange. *J. Vac. Sci. Technol. A* **2018**, *36*, 061504.

(7) Lee, Y.; George, S. M. Thermal Atomic Layer Etching of Al_2O_3, HfO_2, and ZrO_2 Using Sequential Hydrogen Fluoride and Dimethylaluminum Chloride Exposures. *J. Phys. Chem. C* **2019**, *123*, 18455−18466.

(8) Lee, Y.; Huffman, C.; George, S. M. Selectivity in Thermal Atomic Layer Etching Using Sequential, Self-Limiting Fluorination and Ligand-Exchange Reactions. *Chem. Mater.* **2016**, *28*, 7657−7665.

(9) Zywotko, D. R.; Faguet, J.; George, S. M. Rapid Atomic Layer Etching of Al_2O_3 Using Sequential Exposures of Hydrogen Fluoride and Trimethylaluminum With No Purging. *J. Vac. Sci. Technol. A* **2018**, *36*, 061508.

(10) Murdzek, J. A.; Rajashekhar, A.; Makala, R. S.; George, S. M. Thermal Atomic Layer Etching of Amorphous and Crystalline Al_2O_3 Films. *J. Vac. Sci. Technol. A* **2021**, *39*, 042602.

(11) Murdzek, J. A.; George, S. M. Effect of Crystallinity on Thermal Atomic Layer Etching of Hafnium Oxide, Zirconium Oxide, and Hafnium Zirconium Oxide. *J. Vac. Sci. Technol. A* **2020**, *38*, 022608.

(12) Osakada, K. Transmetalation. In *Current Methods in Inorganic Chemistry*; Kurosawa, H., Yamamoto, A., Eds.; Elsevier: 2003; Vol. *3*, Chapter 5, pp 233−291.

(13) Lee, Y.; Johnson, N. R.; George, S. M. Thermal Atomic Layer Etching of Gallium Oxide Using Sequential Exposures of HF and Various Metal Precursors. *Chem. Mater.* **2020**, *32*, 5937−5948.

(14) Johnson, N. R.; Hite, J. K.; Mastro, M. A.; Eddy, C. R.; George, S. M. Thermal Atomic Layer Etching of Crystalline GaN Using Sequential Exposures of XeF_2 and BCl_3. *Appl. Phys. Lett.* **2019**, *114*, 243103.

(15) Walsh, R. Bond-Dissociation Energy Values in Silicon-Containing Compounds and Some of Their Implications. *Acc. Chem. Res.* **1981**, *14*, 246−252.

(16) Lii-Rosales, A.; Cavanagh, A. S.; Fischer, A.; Lill, T.; George, S. M. Spontaneous Etching of Metal Fluorides Using Ligand-Exchange Reactions: Landscape Revealed by Mass Spectrometry. *Chem. Mater.* **2021**, *33*, 7719−7730.

(17) Ban, V. S.; Gilbert, S. L. Chemistry and Transport Phenomena of Chemical Vapor Deposition of Silicon from $SiCl_4$. *J. Cryst. Growth* **1975**, *31*, 284−289.

(18) Bloem, J.; Claassen, W. A. P.; Valkenburg, W. Rate-Determining Reactions and Surface Species in CVD Silicon. 4. The $SICl_4$-H_2-N_2 and the $SiHCl_3$-H_2-N_2 System. *J. Cryst. Growth* **1982**, *57*, 177−184.

(19) Sone, H.; Kaneko, T.; Miyakawa, N. In Situ Measurements and Growth Kinetics of Silicon Carbide Chemical Vapor Deposition from Methyltrichlorosilane. *J. Cryst. Growth* **2000**, *219*, 245−252.

(20) Lemieux, J. M.; Zhang, J. S. Thermal Decomposition of Methyltrichlorosilane, Dimethyldichlorosilane and Methyldichlorosilane by Flash Pyrolysis Vacuum Ultraviolet Photoionization Time-of-Flight Mass Spectrometry. *Eur. J. Mass Spectrom.* **2014**, *20*, 409−417.

(21) Lee, C.; Yang, W.; Parr, R. G. Development of the Colle-Salvetti Correlation-Energy Formula into a Functional of the Electron Density. *Phys. Rev. B* **1988**, *37*, 785−789.

(22) Weigend, F.; Ahlrichs, R. Balanced Basis Sets of Split Valence, Triple Zeta Valence and Quadruple Zeta Valence Quality for H to Rn: Design and Assessment of Accuracy. *Phys. Chem. Chem. Phys.* **2005**, *7*, 3297−3305.

(23) Scuseria, G. E.; Janssen, C. L.; Schaefer, H. F., III An Efficient Reformulation of the Closed-Shell Coupled Cluster Single and Double Excitation (CCSD) Equations. *J. Chem. Phys.* **1988**, *89*, 7382−7387.

(24) Scuseria, G. E.; Schaefer, H. F., III Is Coupled Cluster Singles and Doubles (CCSD) more Computationally Intensive than Quadratic Configuration Interaction (QCISD)? *J. Chem. Phys.* **1989**, *90*, 3700−3703.

(25) Dunning, T. H., Jr.; Hay, P. J. *Modern Theoretical Chemistry*; Plenum: New York, 1977.

(26) Dill, K. A.; Bromberg, S. *Molecular Driving Forces: Statistical Thermodynamics in Biology, Chemistry, Physics and Nanoscience*; Garland Science: 2011.

(27) Frisch, M. J.; Trucks, G. W.; Schlegel, H. B.; Scuseria, G. E.; Robb, M. A.; Cheeseman, J. R.; Scalmani, G.; Barone, V.; Petersson, G. A.; Nakatsuji, H.; et al. *Gaussian 16*, Rev. C.01; Gaussian Inc.: Wallingford, CT, 2016.
(28) Houle, F. A. Electron Impact Fragmentation of Gases by Molecular Beam Mass Spectrometery. Application to $AsCl_3$ and a $GaCl_3/Ga_2Cl_6$ Mixture. *Int. J. Mass Spectrom. Ion Processes* **1993**, *123*, 243−252.
(29) Basner, R.; Gutkin, M.; Mahoney, J.; Tarnovsky, V.; Deutsch, H.; Becker, K. Electron-Impact Ionization of Silicon Tetrachloride ($SiCl_4$). *J. Chem. Phys.* **2005**, *123*, 054313.
(30) Dibeler, V. H.; Mohler, F. L. Dissociation of SF_6, CF_4, and SiF_4 by Electron Impact. *J. Res. Natl. Bur. Stand.* **1948**, *40*, 25−29.
(31) Brunetti, B.; Piacente, V.; Scardala, P. Vapor Pressures of Gallium Trifluoride, Trichloride, and Triiodide and Their Standard Sublimation Enthalpies. *J. Chem. Eng. Data* **2010**, *55*, 98−102.
(32) Zywotko, D. R.; George, S. M. Thermal Atomic Layer Etching of ZnO by a "Conversion-Etch" Mechanism Using Sequential Exposures of Hydrogen Fluoride and Trimethylaluminum. *Chem. Mater.* **2017**, *29*, 1183−1191.
(33) Matsumoto, K.; Kiba, N.; Takeuchi, T. Direct Analysis of Metal Halides by Electron Impact Mass Spectrometry. *Anal. Chem.* **1971**, *43*, 1691.
(34) Palko, A. A.; Ryon, A. D.; Kuhn, D. W. The Vapor Pressures of Zirconium Tetrachloride and Hafnium Tetrachloride. *J. Phys. Chem.* **1958**, *62*, 319−322.
(35) *NIST Chemistry WebBook*. https://webbook.nist.gov/chemistry (accessed 2022-5-28).
(36) Berthold, H. J.; Groh, G. Preparation of Tetramethylzirconium, $Zr(CH_3)_4$. *Angew. Chem., Int. Ed. Engl.* **1966**, *5*, 516−516.
(37) Zywotko, D. R.; Zandi, O.; Faguet, J.; Abel, P. R.; George, S. M. ZrO_2 Monolayer as a Removable Etch Stop Layer for Thermal Al_2O_3 Atomic Layer Etching Using Hydrogen Fluoride and Trimethylaluminum. *Chem. Mater.* **2020**, *32*, 10055−10065.
(38) Stull, D. R. Vapor Pressure of Pure Substances - Organic and Inorganic Compounds. *Ind. Eng. Chem.* **1947**, *39*, 517−550.
(39) Brunetti, B.; Piacente, V.; Scardala, P. A Torsion Study on the Sublimation Process of $InCl_3$. *J. Chem. Eng. Data* **1998**, *43*, 101−104.
(40) Keneshea, F. J.; Cubicciotti, D. Vapor Pressures of Zinc Chloride and Zinc Bromide and Their Gaseous Dimerization. *J. Chem. Phys.* **1964**, *40*, 191−199.
(41) Tangri, R. P.; Bose, D. K. Vapor-Pressure Measurement of Zirconium Chloride and Hafnium Chloride by the Transpiration Techniuque. *Thermochim. Acta* **1994**, *244*, 249−256.
(42) Kabesh, A.; Nyholm, R. S. 716. Studies in Co-ordination Chemistry. Part X. The Vapour Pressure and Heats of Vaporisation of the Stannic Halides. *J. Chem. Soc. (Resumed)* **1951**, 3245−3252.

https://doi.org/10.1021/acs.chemmater.2c01603
Chem. Mater. 2022, 34, 8641−8653